Magic Numbers in Silicon Dioxide-Based Clusters

Can Xu,[†,‡] Wenning Wang,[§] Wingham Zhang,[†,‡] Jun Zhuang,[†,‡] Lei Liu,[†,‡] Qingyu Kong,[†,‡] Li Zhao,[†,‡] Yingcai Long,[§] Kangnian Fan,[§] Shixiong Qian,[†,‡] and Yufen Li*[,†,‡]

State Key Joint Laboratory for Materials Modification by Laser, Ion and Electron Beams, Fudan University, Shanghai 200433, People's Republic of China, Department of Physics, Fudan University, Shanghai 200433, People's Republic of China, and Department of Chemistry, Fudan University, Shanghai 200433, People's Republic of China

Received: July 27, 2000

The generation of magic number silica clusters $[(SiO_2)_nO_2H_3]^-$ with $n = 4$ and 8 by XeCl laser (308 nm) ablation of porous siliceous materials is reported. The production of magic cluster $[(SiO_2)_4O_2H_3]^-$ can be enhanced by sample selection and experimental optimization so that it becomes the most prominent species in silica clusters. To study the structure of the magic cluster $[(SiO_2)_4O_2H_3]^-$, we performed structural optimization for the neutral bare cluster $(SiO_2)_4$, the neutral complex cluster $(SiO_2)_4O_2H_4$, and the anionic cluster $[(SiO_2)_4O_2H_3]^-$ at the HF/6-31G** level. It was found that the ground state of the bare silica tetramer has a linear chain structure whereas a pseudotetrahedral cage-like structural isomer of S_4 symmetry is most stable for the complex cluster $(SiO_2)_4O_2H_4$. The stabilization of the three-dimensional (3D) structure can be attributed to the active participation of the O_2H_4 group in chemical bonding during cluster formation. Our theoretical calculation and bonding analysis indicate that the magic number anionic cluster $[(SiO_2)_4O_2H_3]^-$ might also take a pseudotetrahedral structure similar to (but with a different symmetry) that of the neutral precursor $(SiO_2)_4O_2H_4$ as the ground state in which the valence, coordination, and bonding characteristics of all the constituent atoms are nearly fully satisfied.

1. Introduction

Silica and related materials are of technological importance in manufacturing semiconductors, catalysis, and many other scientific and industrial processes. Siliceous materials have thus been investigated extensively for a long time. Similar to the other materials, siliceous materials at the nanoscale may possess novel properties. An understanding of the structures, stability, and properties of silica nanoparticles and clusters could aid their application to new areas. However, the experimental investigation of SiO_2-based gas-phase clusters and their atomic- and molecular-level descriptions[1−5] have been sparse in the literature, even though cluster science has become quite an active research field[6] in recent decades. This situation might be attributed to the difficulties in SiO_2 cluster generation and in theoretical calculations of large cluster structures. In our recent laser ablation study of silica aerogel, we developed a method for the efficient generation of SiO_2-based clusters,[7] making the experimental study of silica clusters quite feasible. Since then, we have been engaged in a systematic investigation of silica cluster generation from a variety of porous siliceous materials, and many interesting phenomena have been observed.[8−10]

In this paper, we report our recent investigation on the particular silica cluster sequence $[(SiO_2)_nO_2H_x]^-$ generated by XeCl laser (308 nm) ablation of porous siliceous materials, which shows interesting anomalous abundance distribution in its mass spectra. Magic numbers $n = 4$ and 8 have been observed. Magic numbers have attracted a lot of attention in the study of atomic and molecular clusters.[6] The discontinuities in the distribution of cluster intensity versus cluster size in a mass spectrum are usually indications of the special stability of clusters with magic number composition. Such phenomena have been interpreted by the geometric and/or electronic shell structures for rare gas, metal, and other kinds of clusters. Magic numbers also provide insight into the mechanism and energetics of cluster formation processes. Moreover, magic number clusters may often lead to new cluster materials which, if made in bulk quantity under proper conditions, might exhibit novel properties. The most striking examples are Buckminsterfullerene C_{60},[11] MetCars Ti_8C_{12},[12] and the smaller fullerene C_{36}.[13] Thus, the investigation of magic number clusters is of technological as well as fundamental interest. The discovery of magic number silica clusters in our experimental investigation has attracted our particular interest, and related theoretical calculations are carried out to predict their structural, electronic, physical, and chemical properties. As the first step, we performed structural optimization of the neutral bare cluster $(SiO_2)_4$ and the complex cluster $(SiO_2)_4O_2H_4$ at the HF/6-31G** level. From these results, the structures and the bonding characteristics are discussed. On this basis, the structure of the anionic magic silica cluster $[(SiO_2)_4O_2H_3]^-$ is also optimized.

2. Experimental and Computational Methods

The experimental apparatus and techniques have been described in our previous papers.[9,14] An excimer laser was used for generating silica clusters, and time-of-flight mass spectrometry was employed for studying the abundance distribution of the clusters. A variety of porous siliceous materials have been investigated by XeCl laser irradiation at 308 nm. The mass spectrometric measurement was concentrated in the negative

* Corresponding author. E-mail: yfli@srcap.stc.sh.cn. Fax: 86-21-65641344.
† State Key Joint Laboratory for Materials Modification by Laser, Ion and Electron Beams, Fudan University.
‡ Department of Physics, Fudan University.
§ Department of Chemistry, Fudan University.

10.1021/jp002695w CCC: $19.00
Published on Web 10/05/2000

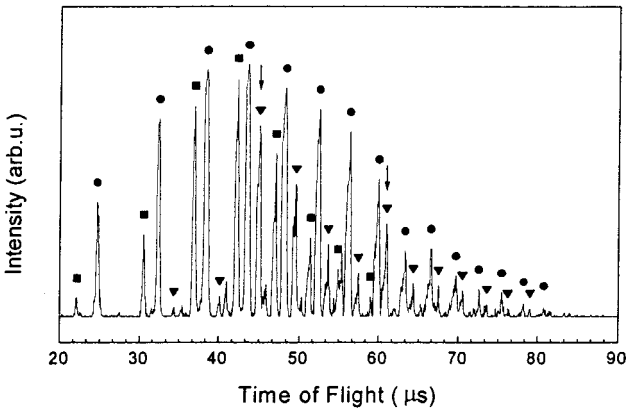

Figure 1. Typical mass spectrum of $[(SiO_2)_nX]^-$ cluster anions obtained by the XeCl excimer laser ablation of Rhodamine 6G-doped silica aerogel. The arrows indicate the magic number $[(SiO_2)_nO_2H_3]^-$ clusters at $n = 4$ and 8. (■) $[(SiO_2)_n]^-/[(SiO_2)_nH]^-$, (●) $[(SiO_2)_nO]^-/[(SiO_2)_n$-$OH]^-$, and (▼) $[(SiO_2)_nO_2H_3]^-$.

ion channel because for the silica clusters, rich information has only been obtained in the negative-ion mass spectra. To determine the chemical composition of the magic number cluster sequence, we have also recorded mass spectra on a newly built reflectron TOF mass spectrometer of mass resolution ~1000.

In the theoretical part of this study, we optimize the structures of the bare silica clusters $(SiO_2)_4$ and the complex clusters $(SiO_2)_4O_2H_4$ and $[(SiO_2)_4O_2H_3]^-$ using ab initio molecular orbital techniques to obtain the minimum energy geometries of the clusters. Optimizations are performed through analytic gradient techniques of the program GAUSSIAN 92[15] at the Hartree−Fock level using the 6-31G** basis set. The frequencies calculated at this level are all positive, indicating that the optimized structures represent minima on the potential energy surfaces.

3. Results and Discussion

3.1. Abundance Distribution of Anionic Silica Clusters: Magic Numbers. Under UV excimer laser ablation, the mass spectra of many porous siliceous materials display some general features. In the negative ion channel, several $(SiO_2)_n$-containing cluster sequences $[(SiO_2)_nX]^-$, with X = _, O, OH, O_2H_x, Si, ... (X's are dependent upon the properties of the samples in general and the surface states of the samples in particular) have been observed. Here we focus our attention on the particular cluster sequence $[(SiO_2)_nO_2H_x]^-$, which shows evidence of magic numbers. For most of the samples we studied, $[(SiO_2)_n]^-$ (and/or $[(SiO_2)_nH]^-$) and $[(SiO_2)_nO]^-$ (and/or $[(SiO_2)_nOH]^-$) are the two most prominent sequences (see Figure 1). Although their abundance distributions vary with samples and experimental conditions, the distributions are always normal, i.e., with no noticeable discontinuities in the mass spectra. In contrast, the sequence $[(SiO_2)_nO_2H_x]^-$ always displays anomalous mass abundance patterns, with sharp discontinuities at $n = 4$ and 8, as shown in a typical mass spectrum of Rhodamine 6G-doped silica aerogel in Figure 1. In other words, 4 and 8 are the magic numbers of this cluster sequence. The intensity of this sequence varies greatly with samples and is relatively abundant for SiOH-rich samples, such as doped silica aerogel and some porous amorphous silica samples. But for surface SiOH-deficient samples, such as hydrothermally treated silicalite-1, this sequence practically disappears. Although the intensity of the magic cluster sequence varies with samples, the composition of the magic clusters remains unchanged—that is, x has a definite value for this sequence. Recently, we repeated the laser ablation

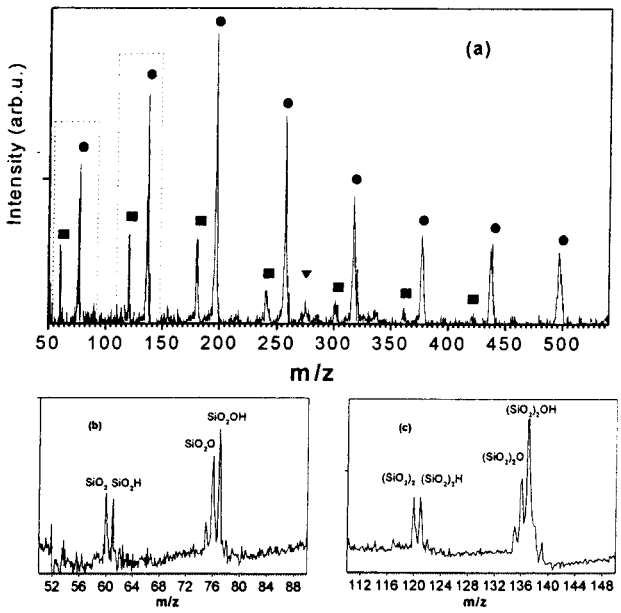

Figure 2. (a) Partial mass spectrum of $[(SiO_2)_nX]^-$ cluster anions obtained by the laser ablation of azo dye-doped xerogel on the reflectron TOF mass spectrometer. (■) $[(SiO_2)_n]^-/[(SiO_2)_nH]^-$, (●) $[(SiO_2)_nO]^-/[(SiO_2)_nOH]^-$, and (▼) $[(SiO_2)_4O_2H_3]^-$. Enlarged plots of the portions depicted in dashed boxes, showing the well-resolved spectra for (b) $n = 1$ and (c) $n = 2$.

experiments of siliceous materials on the reflectron TOF spectrometer, and from the well-resolved mass spectra in which the mass peaks of the $[(SiO_2)_n]^-$ and $[(SiO_2)_nH]^-$ clusters ($n = 1, 2$) and the $[(SiO_2)_nO]^-$ and $[(SiO_2)_nOH]^-$ ($n = 1, 2$) clusters can be clearly discriminated (as illustrated in Figure 2), a value of 3 can be unambiguously assigned to x. From now on, the magic cluster sequence will be designated as $[(SiO_2)_nO_2H_3]^-$.

The most interesting question is whether the abundance of the magic clusters can be effectively enhanced. This has been pursued by sample selection and the optimization of laser ablation conditions. In our previous work, it was found that the mass abundance distribution of the cluster sequences and the maximum cluster size were strongly dependent on the concentration of the surface silanol groups (SiOH) of the siliceous materials.[8−10] That is to say, the surface properties of the samples are of prime importance to the generation of silica clusters. We found that only the SiOH-rich samples are suitable for the generation of the magic number silica clusters. Doped silica aerogels, azodye-doped silica xerogel, and some other porous amorphous silica samples which meet this requirement were studied in our experiments. The laser irradiation conditions also play a very important role in the efficient production of the magic clusters. When medium laser power (600 mJ/cm^2) was used for the laser ablation, the intensity of the $[(SiO_2)_nO_2H_3]^-$ cluster sequence could hardly be recognized at the early stage. When the laser was focused at the same sample site under continuous laser irradiation, the intensity of this sequence gradually increased with irradiation shots, reaching a maximum at 100−120 laser shots and then dropping to nearly zero at 140−160 shots, as shown in Figure 3.

When higher laser power (1000 mJ/cm^2) was applied, the $[(SiO_2)_4O_2H_3]^-$ magic cluster was strikingly enhanced and became even the strongest cluster in the whole mass spectrum, whereas the neighboring clusters with $n = 3$ and 5 remained in their low intensities, indicating the obvious magic characteristics of the $[(SiO_2)_4O_2H_3]^-$ cluster, as illustrated in Figure 4. As we have indicated previously, the maximum attainable cluster sizes

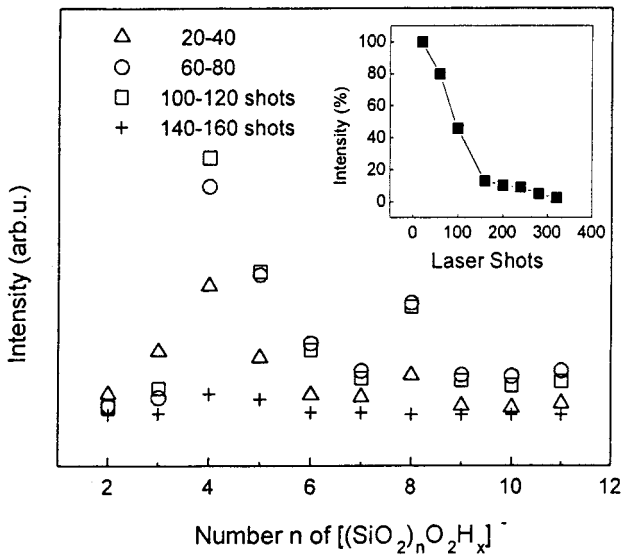

Figure 3. Evolution of the $[(SiO_2)_nO_2H_3]^-$ cluster sequence with the number of laser shots. Inset shows the change of the OH^- concentration with laser shots, normalized by the initial OH concentration.

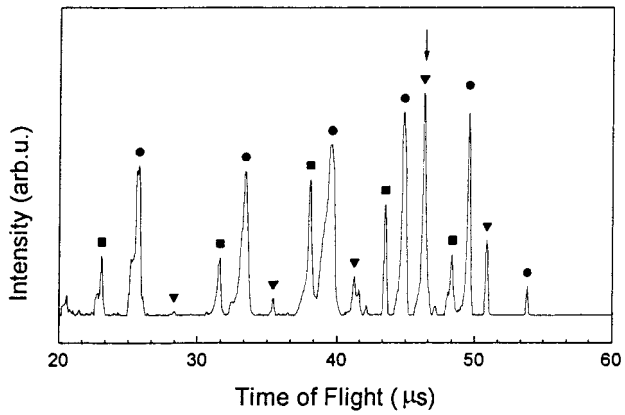

Figure 4. Mass spectrum of $[(SiO_2)_nX]^-$ cluster anions obtained by the XeCl excimer laser ablation of porous amorphous silica at a laser energy of about 1000 mJ/cm^2. The arrow indicates the magic number $[SiO_2)_4O_2H_3]^-$ cluster. (■) $[(SiO_2)_n]^-$/ $[(SiO_2)_nH]^-$, (●) $[(SiO_2)_nO]^-$/ $[(SiO_2)_nOH]^-$, and (▼) $[(SiO_2)_nO_2H_3]^-$.

for all silica cluster sequences decrease with the increasing number of laser shots;[10] under the present conditions, the maximum size had been reduced to $n = 5$ so that the next magic cluster with $n = 8$ did not appear in the spectrum. These preliminary results demonstrate that the generation of the magic number silica cluster can really be greatly enhanced, but for the realization of more efficient production, further experimental exploration is needed.

3.2. Generation Mechanism of the Magic Number Clusters. From our experiments, it is obvious that the formation of the magic number clusters is closely related to the SiOH group of the sample, but the relationship is not simple and clear-cut. Our previous study on the clustering dynamics of silica clusters has revealed a close correlation between the intensities of the $[(SiO_2)_nOH]^-$ sequence and the surface SiOH group of the sample.[9,10] The observation that the formations of both sequences, $[(SiO_2)_nOH]^-$ and $[(SiO_2)_nO_2H_3]^-$, need the presence of the SiOH group of the sample is consistent with the chemical compositions of the clusters, but there must exist a competition between these two sequences, making the growth dynamics very complicated. The inset of Figure 3 shows the change of OH^- concentration in the gas phase with laser irradiation shots. It decreases with laser shots monotonically in a similar way as the intensity of the $[(SiO_2)_nOH]^-$ sequence which was reported in our previous paper.[10] But the intensity of the magic sequence changes quite differently: it increases with laser shots in the early stage and then decreases as shown in Figure 3. Laser-induced annealing caused the decrease of the concentration of SiOH groups of the sample at the laser irradiation region with the accumulation of laser shots. This may be responsible for the intensity evolution of the $[(SiO_2)_nOH]^-$ sequence as well as the magic cluster sequence with laser shots. It seems that the $[(SiO_2)_nOH]^-$ sequence formed first and then part of it transformed into the $[(SiO_2)_nO_2H_3]^-$ sequence. A tentative interpretation of the competition between the two sequences was given below. Laser ablation of the porous silica sample yielded a hole (or pit) at the surface of the sample, which became deeper as the laser was held continuously on the same sample site. The expansion of the laser-induced plasma was slowed by the confinement of the hole. The concentration of OH^- in the plasma within the hole might thus increase with laser shots to some extent at the earlier stage, even though the amount of OH^- generated from the sample surface decreased due to laser annealing. On the basis of the compositions of the clusters, the rate of formation of the $[(SiO_2)_nOH]^-$ sequence is linearly dependent on the OH^- concentration whereas that of the $[(SiO_2)_nO_2H_3]^-$ sequence is nonlinearly dependent (see the discussion on the structure of the $[(SiO_2)_4O_2H_4]$ complex cluster described below). At the beginning of laser ablation, the low OH^- concentration (compared to that accumulated in the hole later) was unfavorable to the formation of the magic cluster sequence so that the $[(SiO_2)_nOH]^-$ sequence appeared first. Then the accumulation of OH^- in the hole accelerated the growth of the magic sequence, leading to its gradual preponderance over the $[(SiO_2)_nOH]^-$ sequence. At this moment, the competition process resulted in the growth of the $[(SiO_2)_nO_2H_3]^-$ magic sequence at the expense of the $[(SiO_2)_nOH]^-$ sequence. Finally, when the surface SiOH groups at the irradiated site were totally ablated by laser annealing, the magic cluster sequence died out. This might be a possible scenario of the growth and competition of the two OH-containing cluster sequences. But the details of the real dynamics remain an unknown; if revealed, they will be helpful in the efficient generation of magic number clusters.

3.3. Theoretical Modeling. The typical mass spectrum in Figure 1 suggests that the $[(SiO_2)_nO_2H_3]^-$ clusters with $n = 4$ and 8 are relatively stable magic clusters. The normal abundance distribution of the $[(SiO_2)_n]^-$ bare silica cluster sequence leads us to the speculation that the group of atoms consisting of 2 O's and 3 H's (not necessarily as a single group) is actively involved in chemical bonding to stabilize the magic clusters. It is well-known that the determination of the structure of gas-phase clusters is a very difficult problem in experimental cluster physics, especially for such complex clusters; no experimental information about the structures of our newly observed magic clusters can be obtained at present or even in the near future. Therefore, we resort to theoretical modeling and calculation when investigating the structures and stabilities of these clusters.

It was found that small silicon oxide clusters Si_xO_y have different types of structures depending on the silicon oxygen ratio.[5] For a cluster with definite composition, there exist many possible structural isomers with different stabilities. Several lower-energy isomers of different symmetries have been found for the silica tetramer $(SiO_2)_4$ and other small silica clusters by theoretical calculation. The problem becomes more complicated for the complex clusters such as the magic number clusters

TABLE 1: Theoretical Calculations of the $(SiO_2)_4$ Structural Isomers at the Hartree−Fock/6-31G* Level

	sym-metry	ZPE (kcal/mol)	*E*(RHF) (Hartree)	ZPE + *E*(RHF) (Hartree)
(a) linear chain	D_{2h}	27.42094	−1755.056238	−1755.012540
(b) double-ring	C_{2v}	26.87185	−1755.029375	−1754.986551
(c) 3D bowl-like	C_{2v}	27.10113	−1754.955790	−1754.912602
(d) ring	D_2	25.72599	−1754.951542	−1754.910545

studied here. As illustrated by many complex ionic clusters,[6] for the $[(SiO_2)_nO_2H_3]^-$ cluster, the atoms of the O_2H_3 group or its negative ion may stay on the surface of the $(SiO_2)_n$ cluster individually or as a whole, or they may be encapsulated inside if the $(SiO_2)_n$ cluster forms a cage. In this paper, we focus our calculation and discussion only on the cluster with $n = 4$. We performed our calculation on the $(SiO_2)_n$ bare silica cluster first and then add the group of atoms to form the complex cluster. Finally, the structure of the anionic magic cluster is studied by proton stripping of the neutral complex cluster.

3.4. Cluster Structures and Bonding Characteristics: $(SiO_2)_4$ and $(SiO_2)_4O_2H_4$. It is known that the ground states of the $(SiO_2)_n$ cluster with $n \leq 3$ have chain structures.[4,16,17] On the basis of their theoretical calculation and photoelectron spectroscopic results, Wang et al.[5] suggested a similar chain structure for the $(SiO_2)_4$ tetramer. However, another previous work on $(SiO_2)_n$ structures by Harkless et al.[18] found a double-ring C_{2v} structure composed of a Si_3O_3 ring and a Si_2O_2 rhombus as the most stable isomer and a linear chain isomer with D_{2h} symmetry and an eight-ring isomer with D_{4h} symmetry as the next two most stable isomers. In their calculations, Harkless et al. used an empirical pairwise interatomic potential to perform the molecular dynamics simulation (the TTAM approximation). Using the same interaction potential, we have performed the structural optimization with the more efficient genetic algorithm and found a cage-like structure of $(SiO_2)_4$ with an energy lower than that of the Harkless ground-state structure.[19] More recently, Nayak et al.,[20] using density functional theory, obtained three lowest-energy isomers of $(SiO_2)_4$, which are the same as those of Harkless but different in their stability order. The calculations of Nayak et al. confirm L. S. Wang's molecular orbital and experimental results, which show that the linear chain isomer is the ground state of the tetramer. Using the 6-31G* basis set at the Hartree−Fock level and taking our genetic algorithm results into consideration, we have identified the four most stable structural isomers of $(SiO_2)_4$. The results are shown in Table 1 and the corresponding structures in Figure 5. In agreement with the results of L. S. Wang and Nayak et al., our ab initio calculations show that the linear chain isomer with D_{2h} symmetry in Figure 5a is the most stable one. The Harkless C_{2v} structure in Figure 5b is the next most stable. As for the eight-ring isomer, our optimization found that the planar eight-ring structural isomer with D_{4h} symmetry discovered by Harkless and Nayak is not the lowest-energy ring isomer; the D_2 ring isomer in Figure 5d is lower in energy. For clarity, we also show a side view of this isomer. In addition, we have found a 3D bowl-like structure with C_{2v} symmetry, as given in Figure 5c, which has not been reported before, and its energy lies between those of the isomers shown in panels b and d of Figure 5. In fact, this bowl-like structure was obtained from the Gaussian optimization of the cage-like structure obtained by genetic algorithms in the TTAM approximation. The change from the cage to the bowl structure demonstrates that the TTAM potential developed for the condensed phase of silica may not be applicable to the studies of small clusters. The relative

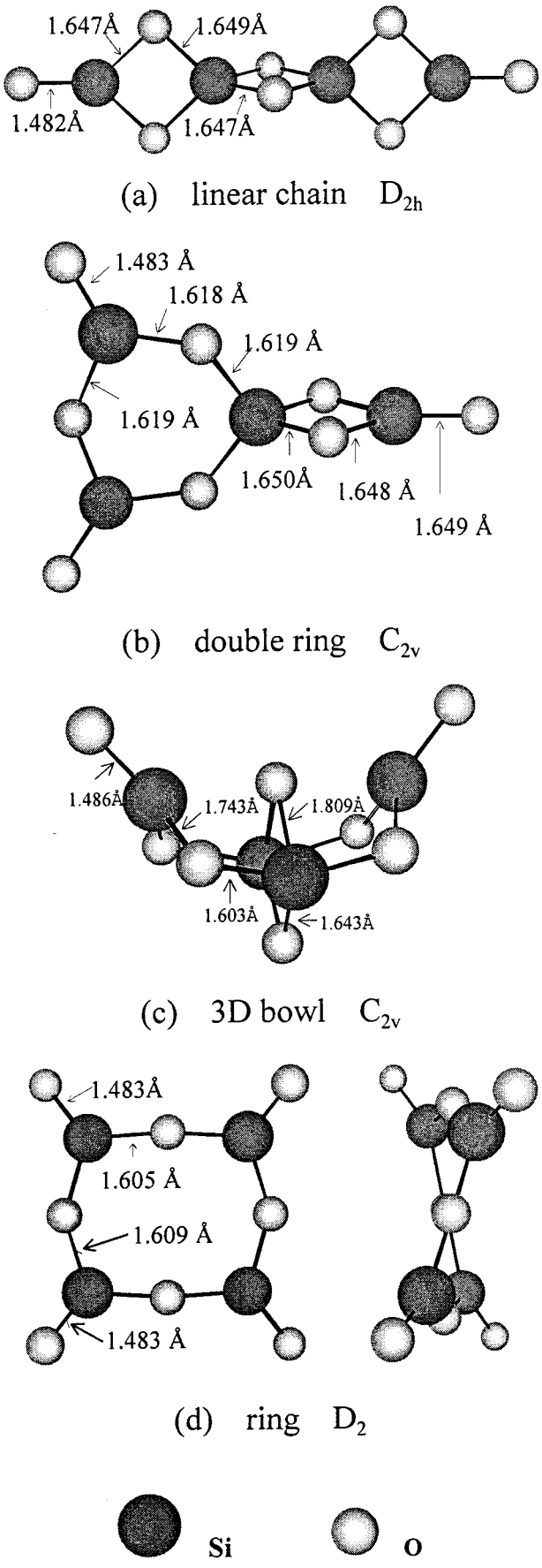

Figure 5. HF/6-31G*-optimized structures of the ground state and the next higher-energy isomers of the neutral $(SiO_2)_4$ cluster: (a) linear chain, D_{2h}, (b) double-ring, C_{2v}, (c) 3D bowl, C_{2v}, and (d) ring, D_2.

TABLE 2: Theoretical Calculations of the $[(SiO_2)_4O_2H_4]$ Structural Isomers at the Hartree−Fock/6-31G Level**

	sym-metry	ZPE (kcal/mol)	*E*(RHF) (Hartree)	ZPE + *E*(RHF) (Hartree)
(a) 3D cage-like	S_4	61.42575	−1907.485747	−1907.387859
(b) linear chain	D_2	61.16557	−1907.376303	−1907.278829
(c) ring	C_2	59.66793	−1907.291352	−1907.196265

stabilities of the a, b, and d isomers of $(SiO_2)_4$ predicted from bonding analysis[20] are consistent with the relative energies of the structures in Table 1. As shown in panels a, b, and d of Figure 5, two, one, and zero Si atoms and six, five, and four O atoms have the preferred 4-fold and 2-fold coordinations, respectively, giving rise to the stability order in the table. As to the bowl-shaped isomer, although two Si and six O atoms have the desired 4-fold and 2-fold coordinations, respectively, just like the coordinations in the linear chain isomer, the tetrahedral bonding of Si is seriously distorted, leading to the lowering of the stability.

For the construction of the $[(SiO_2)_4O_2H_3]^-$ magic number cluster, we first perform our calculation on the corresponding neutral $(SiO_2)_4O_2H_4$ cluster by adding the group of O_2H_4 atoms to the bare silica cluster. The most stable chain structure of $(SiO_2)_4$ was taken as the starting point. The group of O_2H_4 atoms was added as follows: the two terminal Si═O double bonds were broken, one oxygen and two hydrogen atoms were added to each end, and together with the original end O atom, two hydroxyl groups were formed and attached to each of the terminal Si atoms, forming the neutral $(SiO_2)_4O_2H_4$ cluster. In this complex cluster, all the bonding requirements of the Si, O, and H atoms have been satisfied. Next, we construct the magic number cluster structures from the bare $(SiO_2)_4$ isomers c and d. The formation of the ring isomer is similar to the chain case, but here only two of the four Si atoms achieve the preferred 4-fold coordination. The construction of the complex cluster based on the 3D $(SiO_2)_4$ structural isomer is particularly interesting. We find that when the group of O_2H_4 atoms is added to the appropriate positions of the 3D cage structure (before optimization), a beautiful pseudotetrahedral cage-like structure with four hydroxyl groups bound to the four silicon atoms can be formed. In this structure, the valence and the coordination preference of all the constituent atoms and the tetrahedral bonding requirements of the silicon atoms are nearly perfectly satisfied. According to the above bonding analysis, the neutral complex cluster with 3D structure is predicted to have the highest stability, in contrast to the bare $(SiO_2)_4$ cluster. Our calculations of the energies of the structural isomers of $(SiO_2)_4O_2H_4$, formed from the isomer structures of the bare silica cluster in Figure 5 using the 6-31G** basis set at the Hartree−Fock level, confirm our prediction of the stability order. Energy optimization gives the pseudotetrahedral isomer with S_4 symmetry as the ground state of the $(SiO_2)_4O_2H_4$ cluster. The change in stability order from the bare clusters to the complex clusters and the stabilization of the 3D structure can be attributed to the active participation of the group of O_2H_4 atoms in chemical bonding during cluster formation. The energies and corresponding structures of the isomers of the neutral complex clusters are shown in Table 2 and Figure 6, respectively.

To demonstrate the magic characteristics of $(SiO_2)_4O_2H_4$, we have also calculated the energies of the neutral $(SiO_2)_nO_2H_4$ clusters with $n = 3$ and 5. Only the energies of the linear chain isomers are optimized because the stability of the linear chain complex isomer is next to that of the most stable cage-like isomer. The results are given in Table 3. The second energy

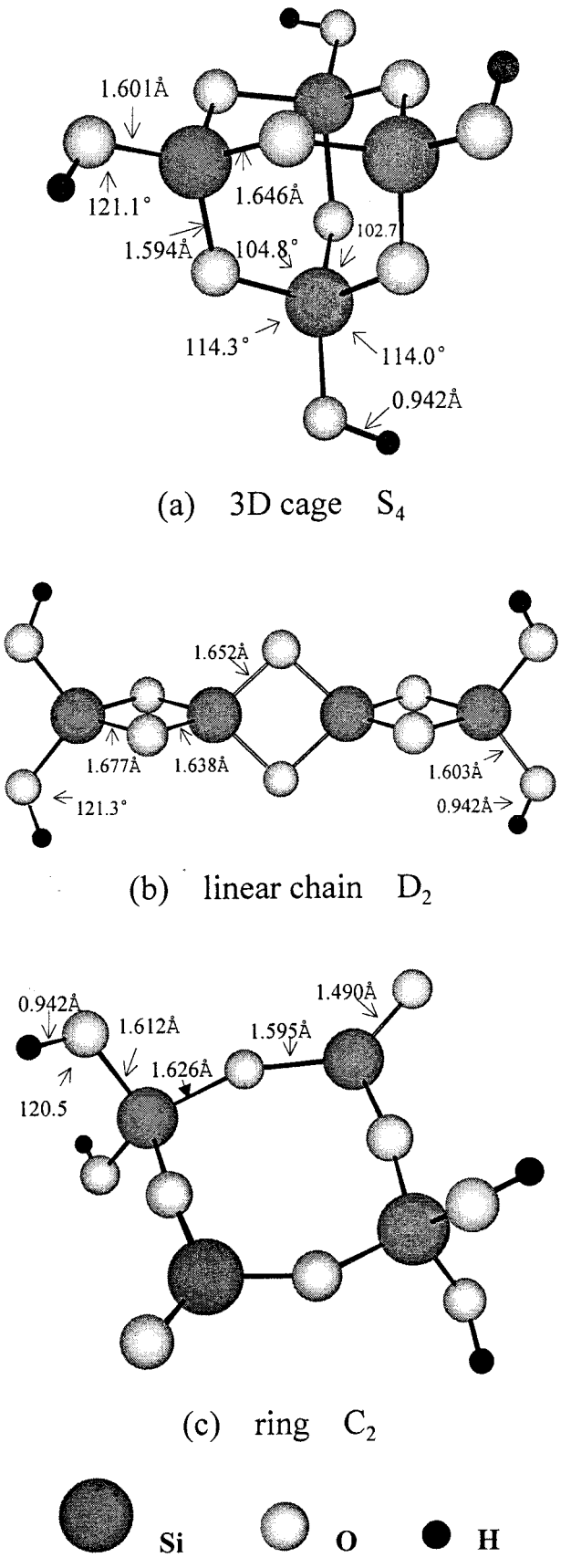

Figure 6. HF/6-31G**-optimized structures of the ground state and the next higher-energy isomers of the neutral $(SiO_2)_4O_2H_4$ complex cluster: (a) 3D cage, S_4, (b) linear chain, D_2, and (c) ring, C_2.

difference calculation indicates that the chain isomers with $n = 3$, 4, and 5 have regular stabilities, i.e., $\Delta E_2 \approx 0$, as shown in eq 1. The $n = 4$ cluster $(SiO_2)_4O_2H_4$ takes the more stable

TABLE 3: Theoretical Calculations of Linear Chain Isomers of $[(SiO_2)_nO_2H_4]$ (n = 3, 4, and 5) at the Hartree−Fock/6-31G Level**

		E(RHF) (Hartree)
linear chain	$[(SiO_2)_3O_2H_4]$	−1468.561346
linear chain	$[(SiO_2)_4O_2H_4]$	−1907.376303
linear chain	$[(SiO_2)_5O_2H_4]$	−2346.195639

TABLE 4: Theoretical Calculations of the Structural Isomers of the Magic Cluster $[(SiO_2)_4O_2H_3]^-$ at the Hartree−Fock/6-31+G Level**

	ZPE (kcal/mol)	E(RHF) (Hartree)	ZPE + E(RHF) (Hartree)
(a) 3D cage-like	54.26529	−1906.960803	−1906.874326
(b) distorted ring	53.51771	−1906.857124	−1906.771838
(c) linear chain	53.70707	−1906.855056	−1906.769468

cage-like structure, whereas the n = 3 and 5 clusters cannot form such structures and remain in the chain structures; the second energy difference ΔE_2 in eq 2 indicates the peculiar stability of the cage-like n = 4 cluster. Therefore, it is clear that the peculiar magic characteristics of the n = 4 cluster originate from its special cage-like structure, in which all the bonding requirements of the constituent atoms can be nearly perfectly satisfied

$$\Delta E_2(\text{chain 3, chain 4, chain 5}) = E_3(\text{chain}) + E_5(\text{chain}) - 2E_4(\text{chain})$$
$$= -0.00438 \text{ au}$$
$$= -0.119 \text{ eV} \quad (1)$$

$$\Delta E_2(\text{chain 3, cage 4, chain 5}) = E_3(\text{chain}) + E_5(\text{chain}) - 2E_4(\text{cage})$$
$$= +0.2145 \text{ au}$$
$$= +5.835 \text{ eV} \quad (2)$$

3.5. Lowest-Energy Structure of the Magic Number Anionic Cluster $[(SiO_2)_4O_2H_3]^-$. To correlate our calculations with the experiments, we deal with the anionic clusters now. For the formation of the anion, electron attachment would give $[(SiO_2)_4O_2H_4]^-$, and proton stripping would give $[(SiO_2)_4O_2H_3]^-$. The latter stoichiometry just matches the experimentally observed composition of the magic number cluster. But the possibility of the existence of the former as a minor species cannot be absolutely excluded. Here we discuss the structure of $[(SiO_2)_4O_2H_3]^-$ only. With the same considerations as mentioned above, we might predict that the anionic magic cluster $[(SiO_2)_4O_2H_3]^-$ would take the distorted pseudotetrahedral cage-like structure of the ground state. Our calculations confirm the prediction. The calculation results and the corresponding structures are given in Table 4 and Figure 7, respectively. The cage-like structure has an energy much lower than those of the chain and the ring isomers. The latter two have nearly the same energies. The ring isomer has its energy lowered through structural distortion, as shown in the figure, but still it cannot compete with the 3D cage structure in stability.

The possibility of the encapsulation of the O_2H_3 group or of its anion in $(SiO_2)_4$ can be ruled out because the optimized structure of the 3D $(SiO_2)_4$ takes the bowl shape instead of the cage.

From our calculation by the HF method at the 6-31+G** level, we come to the conclusion that the magic number $[(SiO_2)_4O_2H_3]^-$ cluster observed in our laser ablation experiments might take the cage-like pseudotetrahedral structure. Its special magic characteristics might be attributed to the peculiar stability of the cage- like structure, the symmetry of which has been changed from the S_4 of the corresponding neutral cluster to C_3 through H^+ stripping.

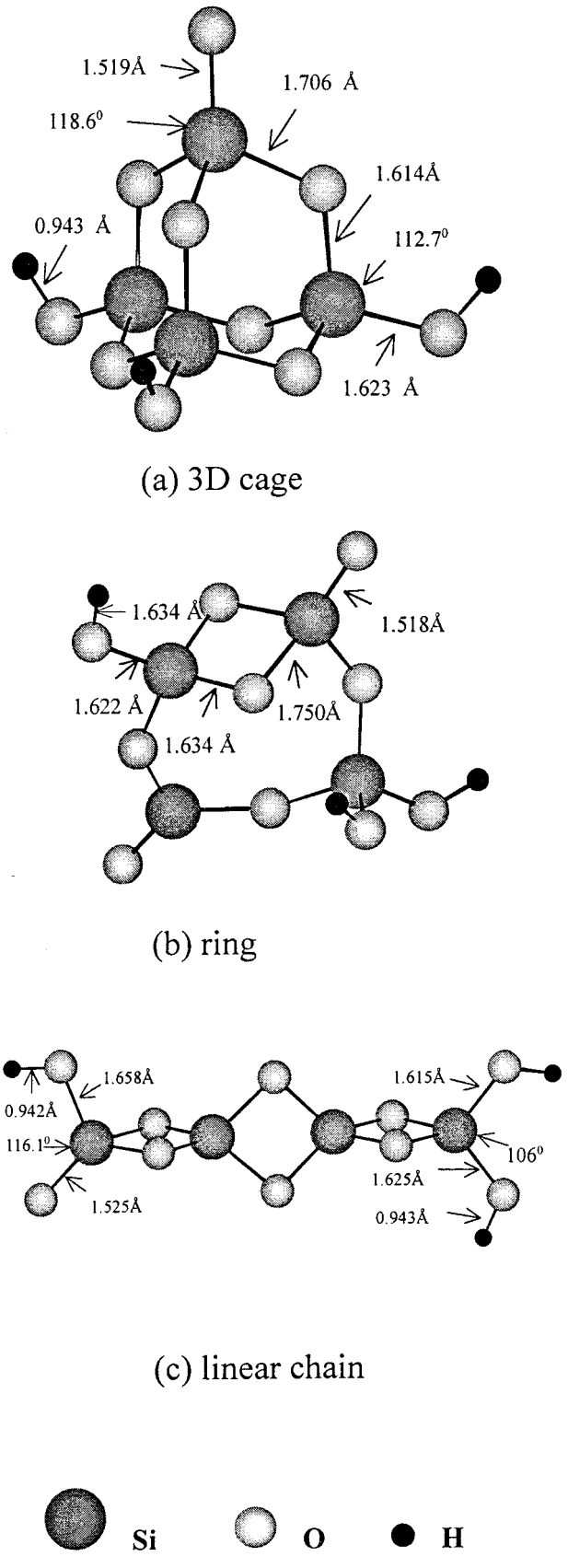

Figure 7. HF/6-31+G**-optimized structures of the ground state and the next higher-energy isomers of the anionic $[(SiO_2)_4O_2H_3]^-$ complex cluster: (a) 3D cage, (b) distorted ring, and (c) linear chain.

The prediction of the structure of the next magic number $[(SiO_2)_8O_2H_3]^-$ cluster is a challenging task. Considering the bonding requirements of all atoms in $[(SiO_2)_8O_2H_3]^-$ and the ground-state structure of the first magic number cluster in the sequence, we have suggested a possible structure for the $n = 8$ neutral $(SiO_2)_8O_2H_4$ cluster, which is composed of two pseudotetrahedral $n = 4$ structural units connected through oxygen bridges. The structure of this cluster has also been optimized. The lack of experimental information prevents verifying our prediction of the structures of these two magic number clusters. Furthermore, since no magic number clusters with $n > 8$ have been observed in our experiments, it is difficult to discuss the growth pattern of the magic cluster sequence. Further experimental and theoretical studies on magic number silica clusters are in progress.

4. Conclusion

New magic number $[(SiO_2)_nO_2H_3]^-$ clusters with $n = 4$ and 8 have been observed in the XeCl excimer laser ablation of porous siliceous samples for the first time. The production of the magic $[(SiO_2)_4O_2H_3]^-$ cluster can be enhanced by optimization of sample and experimental conditions. Theoretical calculations indicate that the anionic magic number $[(SiO_2)_4O_2H_3]^-$ cluster might have the pseudotetrahedral structure in which the valence, coordination, and tetrahedral bonding characteristics are nearly fully satisfied. This pseudotetrahedral structure might also be the structure units of the higher magic number clusters.

Acknowledgment. This work is supported by the National Natural Science Foundation of China (Grants 69608003 and 29890216) and the Shanghai Research Center for Applied Physics (Grant 97JC14018). The authors gratefully acknowledge Prof. Wang Jue and his colleagues at Tongji University for providing the Rhodamine 6G-doped silica aerogel sample.

References and Notes

(1) Jeong, S.; Fisher, K. J.; Howe, R. F.; Willett, G. D. *Microporous Mater.* **1995**, *4*, 467.
(2) Fan, J.; Nicholas, J. B.; Price, J. M.; Colson, S. D.; Wang, L. S. *J. Am. Chem. Soc.* **1995**, *117*, 5417.
(3) Wang, L. S.; Wu, H.; Desai, S. R.; Fan, J.; Colson, S. D. *J. Phys. Chem.* **1996**, *100*, 8697.
(4) Wang, L. S.; Nicholas, J. B.; Dupuis, M.; Wu, H.; Colson, S. D. *Phys. Rev. Lett.* **1997**, *78*, 4450.
(5) Wang, L. S.; Desai, S. R.; Wu, H.; Nicholas, J. B. *Z. Phys. D* **1997**, *40*, 36.
(6) Castleman, A. W., Jr.; Bowen, K. H., Jr. *J. Phys. Chem.* **1996**, *100*, 12911.
(7) Zhao, L.; Zhu, L.; Zhang, J.; Li, Y.; Sheng, J.; Zhang, B.; Wang, J. *Chem. Phys. Lett.* **1996**, *255*, 142.
(8) Xu, C.; Zhang, R.; Zhu, L.; Zhao, L.; Qian, S.; Li, Y.; Long, Y. *Chem. J. Chin. Univ.* **1997**, *18*, 943.
(9) Xu, C.; Long, Y.; Zhang, R.; Zhao, L.; Qian, S.; Li, Y. *Appl. Phys. A* **1998**, *66*, 99.
(10) Xu, C.; Wang, L.; Zhao, L.; Qian, S.; Wang, Z.; Li, Y. *Chem. Phys. Lett.* **1997**, *281*, 426.
(11) Kroto, H. W.; Heath, J. R.; O'Brien, S. C.; Curl, R. F.; Smalley, R. E. *Nature* **1985**, *318*, 162.
(12) Guo, B. C.; Kerns, K. P.; Castleman, A. W., Jr. *Science* **1992**, *255*, 1411.
(13) Piskoti, C.; Yarger, J.; Zettl, A. *Nature* **1998**, *393*, 771.
(14) Zhu, L.; Wang, S.; Wang, P.; Chen, K.; Li, Y. *Chin. Phys. Lett.* **1992**, *9*, 670.
(15) Frisch, M. J.; Trucks, G. W.; Head-Gordon, M.; Gill, P. M. W.; Wong, M. W.; Foresman, J. B.; Johnson, B. G.; Schlegel, H. B.; Robb, M. A.; Replogle, E. S.; Gomperts, R.; Andres, J. L.; Raghavachari, K.; Binkley, J. S.; Gonzalez, C.; Martin, R. L.; Fox, D. J.; Defrees, D. J.; Baker, J.; Stewart, J. J. P.; Pople, J. A. *GAUSSIAN 92*, Revision A; Gaussian Inc.: Pittsburgh, PA, 1992.
(16) Pacansky, J.; Hermann, K. *J. Chem. Phys.* **1978**, *69*, 963.
(17) Mehner, T.; Gocke, H. J.; Schunck, S.; Schnockel, H. *Z. Anorg. Allg. Chem.* **1990**, *580*, 121.
(18) Harkless, J. A. W.; Stillinger, D. K.; Stillinger, F. H. *J. Phys. Chem.* **1996**, *100*, 1098.
(19) Wang, C.; Liu, L.; Li, Y. *Acta Phys.-Chim. Sin.* **1999**, *15*, 139.
(20) Nayak, S. K.; Rao, B. K.; Khanna, S. N.; Jena, P. *J. Chem. Phys.* **1998**, *109*, 1245.